Langmuir
Article
pubs.acs.org/Langmuir

Size Segregation in Sheared Two-Dimensional Polydisperse Foam

Hadi Mohammadigoushki[†] and James J. Feng[*,†,‡]

[†]Department of Chemical and Biological Engineering, University of British Columbia, Vancouver, British Columbia V6T 1Z3, Canada
[‡]Department of Mathematics, University of British Columbia, Vancouver, British Columbia V6T 1Z2, Canada

ABSTRACT: We report experiments on simple shear of a monolayer of bidisperse and polydisperse bubbles in a Couette device. The bubbles segregate according to their sizes, with larger ones in the middle of the gap and smaller ones closer to the walls, when the shear rate and the bubble size ratio are each above a threshold. The spatial distribution of the larger bubbles becomes flatter across the gap as its area fraction increases. To explain these observations, we adapt a model for monodisperse emulsions that predicts the spatial distribution of droplets as an outcome of the competition between migration away from the walls and shear-induced diffusion. The dense packing of bubbles in our foam intensifies bubble−bubble interaction, which manifests itself both in lateral migration due to wall repulsion and in collision-induced diffusion. After accounting for this difference via an effective capillary number based on the deformation of the bubbles, the model predicts the observed bubble distributions accurately.

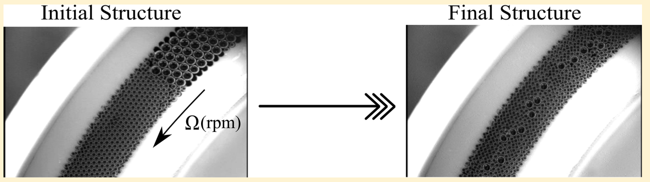

1. INTRODUCTION

Liquid foams are a concentrated dispersion of gas bubbles in surfactant solutions and exhibit complex flow behavior and rheology.[1−6] It is widely recognized that such complex dynamics is rooted in the foam's microstructure on the bubble scale; the bubbles may undergo breakup, coalescence, coarsening, and morphological changes.[7−12] Prior experiments have indicated the possibility that bubbles may segregate according to size in a flowing polydisperse foam, but other experiments suggested evidence to the contrary. Herzhaft[13] sheared three-dimensional (3D) polydisperse foams between parallel disks and reported that the large bubbles tend to appear at the middle of the gap while smaller ones are closer to the walls. One explanation is that the bubbles have segregated according to size during the shear. However, an alternative is bubble breakup[14] and coalescence[15] under shear, which could also have produced the observed patterns. In an experiment designed expressly to probe bubble migration, Quilliet et al.[16] produced a monolayer of monodisperse bubbles as a two-dimensional (2D) foam and inserted a bubble larger than its neighbors. Under oscillatory shear, the large bubble is seen to migrate toward one of the boundaries of the cell. This is inconsistent with Herzaft's report of migration away from walls. In a Hele−Shaw cell, Cantat et al.[17] reported aggregation of large bubbles among smaller neighbors. Cox et al.[18,19] studied planar extension of bidisperse 2D foams experimentally and numerically and found no sign of size-based bubble segregation. Therefore, the question of size segregation in flowing polydisperse foam remains open.

For emulsions and suspensions, on the other hand, the segregation and margination of drops and particles are well documented in confined flows.[20−23] For example, bidisperse suspensions of particles show mild size segregation in 2D channel flow.[20,21] White blood cells and platelets are found closer to the walls while red cells aggregate in the center of the tube.[22,23] We should note of course that foams are different from suspensions or emulsions in that the bubbles are closely packed, with relatively little suspending fluid in between. Thus, they have a much reduced mobility.

In a recent study, we have taken the first step toward answering the question of size segregation in sheared foam by studying the migration of a single large bubble in an otherwise monodisperse bubble raft.[24] In a Couette shear cell, we saw migration of the large bubble away from the walls toward the center of the gap, apparently driven by a "wall repulsion". This appears consistent with the observations of Herzhaft[13] but not those of Quilliet et al.[16] Now in bidisperse and polydisperse foams, a new factor is that the large bubbles interact among themselves as well. How does this interaction affect the migration of the bubbles of different sizes? Do bubbles segregate based on size, and if yes, what is the role of the area fraction of different species? These are the questions we set out to answer.

2. MATERIALS AND METHODS

We conduct experiments with a monolayer of bubbles resting on the top of a soap solution. In comparison with 3D foams, such a 2D foam offers direct visualization of the bubbles and thus has been the preferred setup in recent studies on structural changes of sheared foams.[6,12,15,19] The soap solution is a mixture of distilled water (15 wt %), glycerine (Fisher Scientific, 80 wt %), and dish washing liquid (Sunlight by Unilever, 5 wt %). The experiments were performed in a modified Couette device with a rotating sharp-edged inner disk of radius R_1 = 9.3 cm and a stationary outer cylinder of inner radius R_2 = 10 cm. By injecting nitrogen through an immersed needle in the soap solution, we make bubbles of highly uniform and controlled sizes. A high bulk surfactant concentration, c = 5 wt %, about 100 times the critical micelle concentration, is used to prevent the bubbles from bursting.[15] The experiments are carried out at room temperature. The soap solution has a Newtonian viscosity μ = 50

Received: November 7, 2012
Revised: December 24, 2012
Published: January 7, 2013

$\pm$ 2 mPa·s, a density ρ = 1200 kg/m^3, and a surface tension σ = 25 $\pm$ 2 mN/m. The experimental setup and material characterizations are similar to our earlier experiments,[15,24] and more details can be found there. By using a highly viscous suspending liquid, we ensure a Newtonian linear velocity profile in the narrow gap $d = R_2 - R_1$ = 7 mm, with a uniform shear rate $\dot{\gamma} = \Omega R_1/d$, where Ω is the rotation rate of the inner cylinder. In the narrative below, we will use both Ω and $\dot{\gamma}$, with $\dot{\gamma}$ (s^{-1}) $\approx$ 1.39Ω (rpm) for our device. We will report results on 15 bidisperse and polydisperse foam samples, and their bubble sizes and area fractions are listed in Table 1. Note that Φ_i values are the background area fractions averaged over the entire foam, namely, the total area occupied by bubbles of radius a_i divided by the whole area of the bubble raft. It is not to be confused with the spatially varying, *local* area fractions ϕ_i that are the key observables of the experiment.

Table 1. Composition of the Bidisperse and Polydisperse Foam Samples Used in the Experiments[a]

sample	Φ_1 (%)	Φ_2 (%)	Φ_3 (%)	Φ_4 (%)
Bidisperse				
A	80	20	—	—
B	95	—	5	—
C	90	—	10	—
D	80	—	20	—
E	70	—	30	—
F	50	—	50	—
G	80	—	—	20
Polydisperse				
H	90	5	5	—
I	80	10	10	—
J	60	20	20	—
K	40	30	30	—
L	90	—	5	5
M	80	—	10	10
N	60	—	20	20
O	40	—	30	30

[a] Φ_1, Φ_2, Φ_3, and Φ_4 are the area fractions of the bubble species with radii a_1 = 350 μm, a_2 = 500 μm, a_3 = 700 μm, and a_4 = 875 μm, respectively.

3. EXPERIMENTAL RESULTS AND DISCUSSION

It turns out that the key features of size-based segregation are mostly manifested in bidisperse foams already. For ease of analysis, therefore, we will focus on bidisperse foams in the following, with a final subsection devoted to features specific to polydisperse ones.

3.1. Size Segregation in Bidisperse Foam. Figure 1 illustrates a typical process of size-based segregation of the two bubble species under shear. The distribution of the large bubbles, of radius a_3 = 700 μm in this case, are generated by averaging over several snapshots taken in repeated experiments. In each snapshot, we divide the visible domain of the foam into nine parallel strips of equal thickness across the gap d and count the number of large bubbles in each strip. This produces a profile of the area fraction for the large bubbles, $\phi_3(y)$, normalized by the average fraction Φ_3 = 20%, with y being the dimensionless coordinate across the gap with the origin at the center and y = $\pm$0.5 at the walls. The large bubbles are initially released close to the walls (Figure 1a). Under a rotational rate Ω = 5 rpm, the two species mix at first (Figure 1b). In time, however, the large bubbles aggregate in the center of the gap, within $|y| < y_e \approx 0.25$ in this case, and a quasi-steady state is reached at t = 5 min (Figure 1c). In this state, there is no statistically significant variation along the azimuthal direction. The quasi-steady distribution of the bubbles is independent of the initial configuration. Figure 2 shows that three different initial distributions at the same Φ_3 = 20% all lead to the same final distribution. Of course, the time required to reach the final state differs. For brevity, we will refer to the quasi-steady state after prolonged shearing simply as the "steady state".

The apparent aggregation of large bubbles at the center of the gap is consistent with our earlier observations on the migration of single large bubbles in a 2D foam of smaller bubbles.[24] To sum up those findings, a large bubble off the center of the gap experiences an asymmetric "bumping force" from the small bubbles that pass along its sides under shear. This produces a "wall repulsion" toward the center of the gap, much as in the migration of a single drop submerged in a suspending liquid.[25,26] Furthermore, the migration speed can be predicted by the Chan–Leal formula[25] if the capillary number C is replaced by an *effective capillary number* C_e that is higher than C and accounts for the enhanced deformation of the large bubble under the continuous impact of the smaller surrounding bubbles. In the present study, the obvious difference is that there are multiple large bubbles that interact among themselves as well. This will be examined in Section 3.3.

There are two prerequisites for the migration of the single large bubble in an otherwise monodisperse foam of smaller

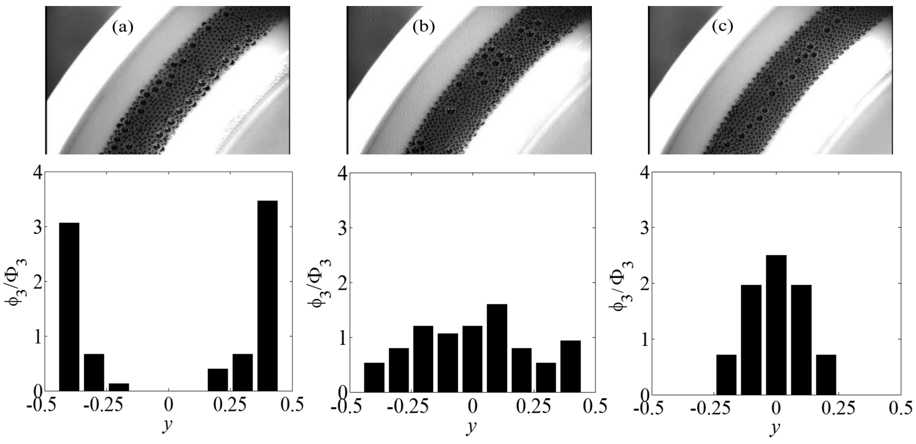

Figure 1. Size segregation in sample D under shear (Ω = 5 rpm). The upper row consists of snapshots of the foam at different times: (a) t = 0; (b) t = 2 min; (c) t = 5 min. The lower row shows the corresponding large bubble distributions $\phi_3(y)/\Phi_3$.

dx.doi.org/10.1021/la304445f | Langmuir 2013, 29, 1370–1378

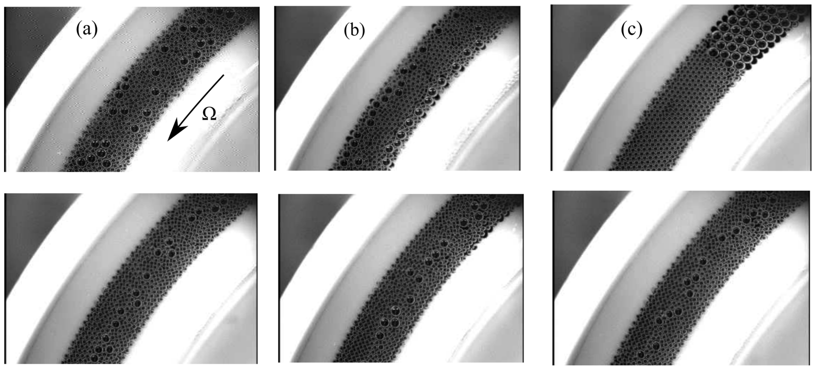

Figure 2. Three different initial configurations of sample D (top row), with the large bubbles randomly distributed (a), near the walls (b), and segregated into azimuthal segments (c), lead to the same quasi-steady distribution in the lower row after shearing at $\Omega = 7$ rpm for 10 min. The arrow indicates the direction of shearing.

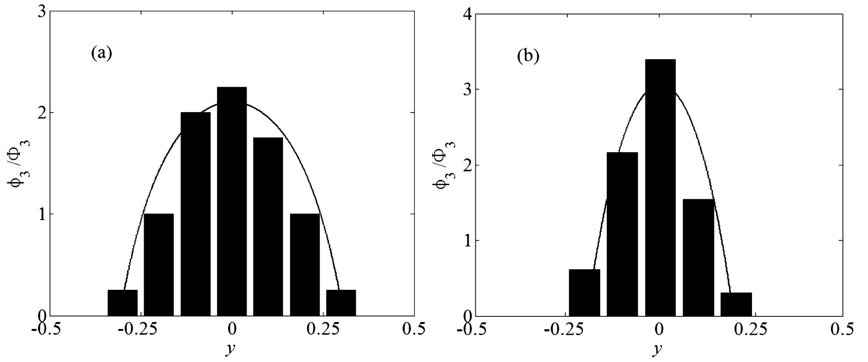

Figure 3. Steady-state distribution of the large bubbles in sample C after shearing at (a) $\Omega = 3$ rpm and (b) $\Omega = 7$ rpm for 10 min. The solid lines are predictions of the migration−diffusion model to be discussed in Section 3.5.

bubbles:[24] that the shear rate $\dot{\gamma}$ and the bubble size ratio κ each be above a certain threshold. These reflect the discreteness of the foam; it takes a minimum force to push a large bubble from one row to the next against the capillary pressure in the neighboring bubbles. Such thresholds have also been observed for the bidisperse foams here. In fact, the two threshold values of Ω and κ are expected to be the same as for a single large bubble.[24] Insofar as they are critical values corresponding to the onset of lateral migration of the large bubbles, they are unaffected by the interaction among large bubbles, which arises only after the thresholds have been crossed. For example, no segregation occurs in sample A for Ω up to 7 rpm, the highest rotational rate without incurring centripetal effects;[24] the bubble size ratio $\kappa = a_2/a_1 = 1.43$ is too small. In sample D ($\kappa = 2$), the threshold is around $\Omega = 3$ rpm. For sample G ($\kappa = 2.5$), it has come down to around 2 rpm. We have previously presented detailed experimental data on the thresholds,[24] along with an analytical expression for the critical condition based on scaling arguments.

3.2. Effect of Shear Rate. The shear rate affects both the final steady-state bubble distribution across the gap and the approach to that steady state. Figure 3 shows the steady-state distribution of a_3 in sample C after shearing at different rotational speeds. Evidently, with increasing shear rate, the final distribution of the large bubbles becomes more narrowly peaked, and the near-wall regions free of large bubbles widen. For the two cases shown, the half-width of the large-bubble distribution $y_e \approx 0.28$ and 0.22 for $\Omega = 3$ and 7 rpm, respectively.

Furthermore, we compare the speed of segregation at different shear rates starting from the same uniform initial configurations. Figure 4 plots the temporal evolution of the half-width of the large-bubble distribution, $y_e(t)$. At higher shear rate, the size segregation proceeds at higher speed, and the steady-state distribution is attained within a shorter time. Intuitively, this trend is reasonable. Faster shearing causes more vigorous and frequent impingement of the small bubbles onto the large ones, which should enhance the speed of lateral migration for the latter. A more precise analysis calls for the introduction of another factor, *shear-induced diffusion* of the large bubbles, which influences the steady-state distribution as well. We will return to this shortly in Section 3.5 with the help of a theoretical model.

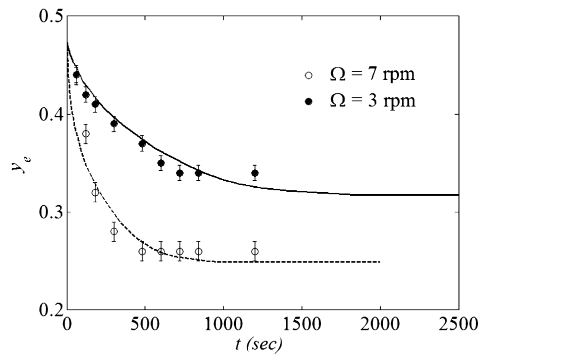

Figure 4. Temporal evolution of the half-width of the large-bubble distribution, $y_e(t)$, for sample D at $\Omega = 3$ and 7 rpm. The solid and dashed lines indicate predictions of the migration−diffusion model.

3.3. Effect of Area Fraction of Large Bubbles. The size segregation in polydisperse foams differs from the migration of a single large bubble studied before[24] in that the large bubbles interact among themselves. Naturally, one expects this

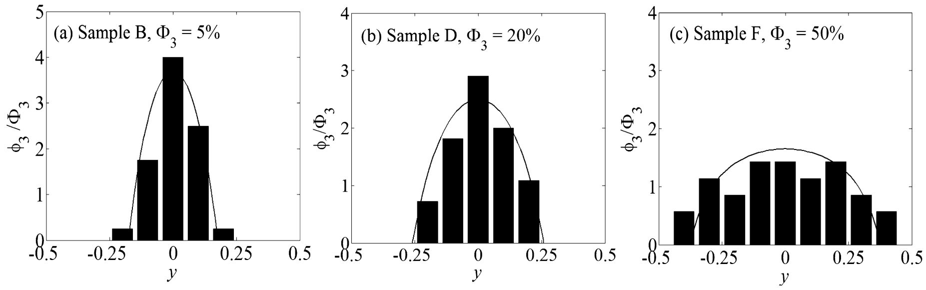

Figure 5. Steady-state distribution of the large bubbles in samples B, D, and F after 10 min of shearing at 7 rpm. These samples have the same bubble sizes but different area fractions for the larger bubbles (see Table 1). The solid lines are predictions of the migration–diffusion model.

interaction to depend on the large-bubble area fraction. By shearing samples B, D, and F, with Φ_3 = 5%, 20%, and 50% for the large bubbles, respectively, we compare the steady-state distributions in Figure 5. By increasing Φ_3, the distribution becomes broader, and the large bubbles are more spread out in the gap. This is a telltale of the interaction among large bubbles producing an *effective diffusion*. At even higher fractions, the large bubbles become essentially uniformly distributed across the gap.

Moreover, Figure 6 compares the temporal development toward the steady state at two different Φ_3 values. For sample E at the higher Φ_3 = 30%, the equilibrium distribution is achieved more rapidly. In view of the wider distribution in equilibrium (Figure 5c), or equivalently the larger steady-state y_e value, the large bubbles initially near the walls need to travel less distance to reach their equilibrium position. This seems to provide an easy rationalization of Figure 6, but a more careful examination will be made below with the help of a quantitative model.

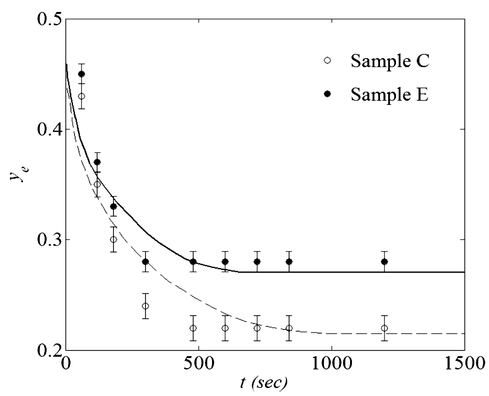

Figure 6. Temporal evolution of $y_e(t)$ for samples C (Φ_3 = 10%) and E (Φ_3 = 30%) undergoing shear at 7 rpm. The solid and dashed lines indicate predictions of the migration-diffusion model.

3.4. Effect of Bubble Size Ratio. As the last "control parameter", we study the effect of the bubble size ratio κ. Figure 7 compares the steady-state distributions and temporal evolution of y_e for two bidisperse foam samples with the same large-bubble area fraction Φ but different κ values. Sample G, with the larger κ, exhibits a more sharply peaked steady distribution and reaches it more rapidly than sample D. This mirrors the effects of the shear rate (cf. Section 3.2). In the migration of a single large bubble in an otherwise monodisperse foam of small bubbles,[24] we have found that a larger κ increases the migration velocity as if by elevating the shear rate. In fact, an effective capillary number C_e can be defined based on κ that quantitatively captures this effect. The model presented below will make a similar connection for the bidisperse foams.

3.5. Migration–Diffusion Model. The description above indicates that size segregation in sheared foam is driven by the *migration due to wall repulsion*, the same mechanism as operates on a single large bubble in a medium of smaller ones.[24] A second key player, one that distinguishes the bidisperse foam from the single-large-bubble scenario, is the interaction among the large bubbles themselves. This interaction may be described by the idea of *shear-induced diffusion* that is familiar from prior studies of suspensions and emulsions.[20,21,27–30] The competition between these two factors determines the speed of segregation between bubbles of different sizes and their final distribution.

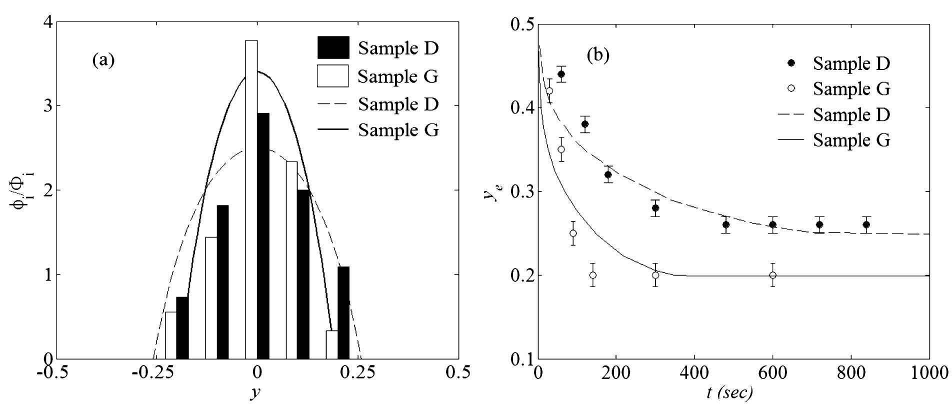

Figure 7. Effect of the bubble size ratio κ on (a) the steady-state distribution of the large bubbles and (b) the transient to the steady state in terms of y_e. Sample D has a bubble size ratio κ = 2, and sample G has κ = 2.5. Both have 20% average area fraction for the large bubbles and are subject to Ω = 7 rpm. The solid and dashed lines represent the model predictions.

dx.doi.org/10.1021/la304445f | *Langmuir* 2013, 29, 1370–1378

King and Leighton[29] and Hudson[30] studied the spatial distribution of drops in sheared dilute monodisperse emulsions and investigated the interplay between wall migration and shear-induced diffusion. The evolution of the drop volume fraction ϕ in a simple shear obeys a convection−diffusion equation:

$$\frac{\partial \phi}{\partial t} = -\frac{\partial}{\partial y'}\left(v_{\mathrm{m}}\phi - D\frac{\partial \phi}{\partial y'}\right) \quad (1)$$

where v_{m} is the velocity of wall-induced migration, D is a diffusivity, and $y' = yd$ is the *dimensional* coordinate across the gap. The Chan−Leal formula[25] is used for v_{m}, in terms of the dimensionless y:

$$v_{\mathrm{m}} = -4\alpha\frac{\sigma}{\eta}\frac{a^2}{d^2}C^2\left[y + \frac{8y}{(1-4y^2)^2}\right] \quad (2)$$

where α is a mildly varying function of the drop-to-matrix viscosity ratio given by Chan and Leal,[25] σ is the interfacial tension, η is the ambient fluid viscosity, a and d are the drop radius and gap size, respectively, and $C = \eta\dot{\gamma}a/\sigma$ is the capillary number. The diffusivity D is written as

$$D = \phi\dot{\gamma}a^2\lambda \quad (3)$$

where λ is a dimensionless coefficient. Balancing the drop fluxes due to wall migration and diffusion, Hudson[30] arrived at the following steady-state profile:

$$\phi(y) = \phi_0 + Pe\left(1 - \frac{y^2}{2} - \frac{1}{1-4y^2}\right) \quad (4)$$

where $\phi_0 = \phi(0)$ is a constant of integration and the Peclet number is

$$Pe = 4\alpha\frac{a}{d}\frac{C}{\Phi\lambda} \quad (5)$$

with Φ being the average volume fraction. Note that both v_{m} and ϕ diverge toward the walls ($y \to \pm 0.5$). The actual profile comprises the positive central part of eq 4 and drop-free layers next to the walls, whose edges ($y = \pm y_{\mathrm{e}}$) are determined by setting $\phi(y_{\mathrm{e}}) = 0$ in eq 4. Conservation of the drop volume $\int_{-y_{\mathrm{e}}}^{y_{\mathrm{e}}} \phi(y)\,\mathrm{d}y = \Phi$ specifies the centerline volume fraction ϕ_0.

To adapt this emulsion model to our bidisperse foam, we make the same analogy as was used previously to represent the wall-induced migration of a single large bubble in a sheared monodisperse foam of smaller bubbles.[24] Essentially, we view the smaller bubbles as constituting an effective continuum that suspends and flows around the large bubbles, playing the role of the continuous-phase liquid in the emulsion. Of course, the foam is 2D while the emulsion is 3D, and the smaller bubbles exert a hydrodynamic impact on the larger ones that differs from that of a continuous, viscous liquid. Most importantly, the large bubbles are observed to deform much more than in a viscous liquid under the same capillary number. Mohammadigoushki and Feng[24] found that the enhanced deformation can be described by an empirical equation for an *effective capillary number*:

$$C_{\mathrm{e}} = C(2.5\kappa^2 - 7\kappa + 11) \quad (6)$$

with κ being the large-to-small bubble size ratio. C_{e} is larger than C and when used in the Taylor formula for drop deformation predicts the observed bubble deformation. With C being replaced by C_{e}, the migration velocity v_{m} of a single large bubble can be predicted accurately by the Chan−Leal formula.[24] This v_{m} can be used in the emulsion model (eq 1) for the bidisperse foam at hand. Then, we need only to find the counterpart of the diffusivity of eq 3.

As far as we know, the idea of shear-induced diffusion has never been used for foams before, and no measured data exist for D or λ. In emulsions, one may consider λ a function of the viscosity ratio, the surface mobility, the capillary number C, and the drop fraction Φ. For surfactant-stabilized dilute emulsions, King and Leighton[29] have reported $\lambda(C)$ as a weakly rising function of the capillary number C (cf. their Figure 8). In surfactant-free emulsions, Hudson[30] obtained λ values that are an order of magnitude larger, owing to the higher surface mobility. Viewed as an emulsion of the large bubbles in an effective liquid medium, our bidisperse foam is similar to King and Leighton's emulsion in that the surfaces are immobilized by surfactants and the drop-to-matrix viscosity ratio is negligibly small. Thus, we borrow their dimensionless diffusivity λ, now as a function of the effective capillary number C_{e}. In fact, all our experiments have used low shear rates such that $C_{\mathrm{e}} < 0.1$, in which range $\lambda = 0.02 \pm 0.002$ remains essentially constant (see Figure 8 of King and Leighton[29]). Therefore, we have simply taken $\lambda = 0.02$ in our model calculations. Note that this neglects any dependence of λ on Φ and possibly also on the bubble size ratio κ in our foam. Both prior experiments[29,30] used dilute emulsions and neither explored the effect of Φ. We assume that λ is independent of the area fraction of the large bubbles for our bidisperse foam. This assumption will be validated a posteriori by comparing the model prediction with experimental data over the whole range of area fraction. With the effective continuum analogy, increasing κ amounts to increasing the effective capillary number C_{e} through eq 6. As long as we operate in the low-C_{e} regime, the κ effect on λ can be safely neglected.

Having λ thus determined and noting that $\alpha = 81/140$ for an emulsion of negligible drop viscosity,[25] we calculate the Peclet number for our bidisperse foam as

$$Pe = \frac{81}{35}\frac{a}{d}\frac{C_{\mathrm{e}}}{\Phi\lambda} \quad (7)$$

With this Peclet number, we can use eq 4 to predict the steady-state distribution of the large bubbles in our bidisperse foam and integrate eq 1 for the transient toward the steady state. In eq 4, the centerline concentration ϕ_0 is determined from the conservation of drop volume $\int_{-y_{\mathrm{e}}}^{y_{\mathrm{e}}} \phi\,\mathrm{d}y = \Phi$. Equation 1 is integrated using finite difference with boundary conditions $\phi(\pm y_{\mathrm{e}}) = 0$, with y_{e} being determined iteratively from the drop volume conservation by the shooting method. Both the steady ϕ profile and the transient can be compared with measurements. In particular, we will examine the effects of the shear rate $\dot{\gamma}$, the average area fraction Φ, and the bubble size ratio κ.

Figure 3 compares the model predictions with the measured steady-state distributions for the bidisperse sample C at two shear rates, and Figure 4 compares the temporal development of the distribution for sample D. In both cases, the rotational speeds of 3 and 7 rpm correspond to capillary numbers $C = 5.8 \times 10^{-3}$ and 1.4×10^{-2}, which in turn correspond respectively to effective capillary numbers $C_{\mathrm{e}} = 4.0 \times 10^{-2}$ and 9.5×10^{-2}. On the basis of these parameters, the predicted steady-state profile and its temporal development are both in reasonably good agreement with experimental measurements. With increasing shear rate, the large bubbles migrate away from the walls more rapidly, and this aggregation at the center overpowers the shear-induced diffusion that strives to spread the large bubbles uniformly. Consequently,

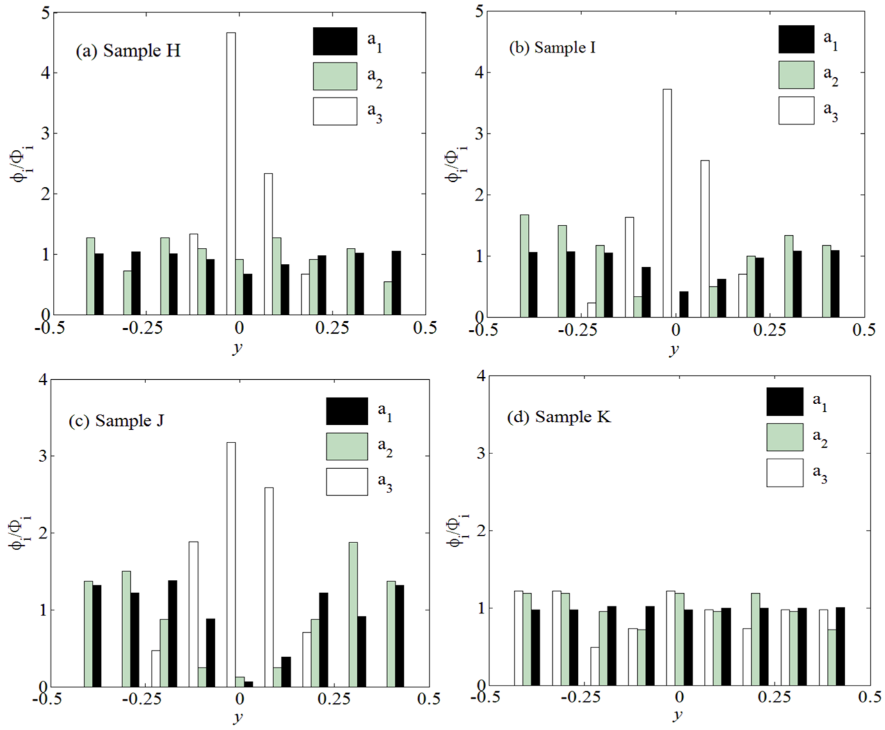

Figure 8. Steady-state bubble distributions in the polydisperse foam samples H, I, J, and K, after 10 min of shearing at 7 rpm. The samples have the same three bubble sizes, $a_1 = 350\ \mu$m, $a_2 = 500\ \mu$m, and $a_3 = 700\ \mu$m, at different average area fractions: (a) sample H, $(\Phi_1, \Phi_2, \Phi_3) = (90\%, 5\%, 5\%)$; (b) sample I, (80%, 10%, 10%); (c) sample J, (60%, 20%, 20%); (d) sample K, (40%, 30%, 30%). The area fractions are normalized for each species.

the size-based segregation occurs more rapidly for higher shear rates and produces a narrower equilibrium distribution centered at the middle of the gap $y = 0$. Note that eq 1 does not predict a $t \sim \dot{\gamma}^{-1}$ scaling for the transient. It would if v_m and D were both proportional to $\dot{\gamma}$ or C. In reality, $v_m \propto C^2$, and D also depends on C nonlinearly thanks to $\lambda(C)$.[29] Our experimental data do not exhibit such a scaling either.

As the average area fraction of the large bubbles Φ_3 increases, Figure 5 shows that the model correctly predicts the widening of the equilibrium distribution and the agreement with measurements is quantitatively accurate. The idea underlying this prediction is that higher fraction of the large bubbles increases the frequency of their collision and thereby elevates the effective diffusivity D (cf. eq 3). This has been confirmed by the experiments. We have also studied the effect of area fraction on the speed of size segregation. The model predicts that, with increasing Φ_3, the segregation occurs more rapidly (Figure 6); it takes less time to reach the equilibrium distribution. This captures the trend in the experimental data if not the precise values of the segregation time. Qualitatively, increasing Φ_3 increases the diffusivity D, which should counteract the migration and lead to a slower segregation. On the other hand, a higher Φ_3 corresponds to a wider equilibrium distribution with a larger y_e. This means that large bubbles initially near the wall need to travel a shorter distance to get to their steady-state position. These two effects oppose each other, and the outcome seems to be in favor of the latter. King and Leighton[29] have quantified the competition between the two effects in the limiting case of small y. By linearizing the migration velocity v_m of eq 2 (i.e., reducing the y terms between the brackets to $9y$), they obtained a self-similar solution in which time t scales only with d/v_m and is independent of Φ_3. Our experiment and analysis are not restricted to the small-y limit and thus do not exhibit the similarity. Recall that we have assumed λ to be independent of Φ in eq 7. The close agreement for the whole range of area fractions studied here indicates that this is a reasonable assumption.

Finally, we examine the effect of the bubble size ratio κ, which influences the structural evolution of bidisperse foams through the $C_e \sim C$ relationship in our model (eq 6). Figure 7 shows that the model correctly predicts the effects of κ on the steady-state distribution as well as on the temporal evolution toward it: higher κ produces a faster approach to a narrower steady-state distribution. Therefore, qualitatively and quantitatively (via eq 6) increasing κ has similar effects to elevating the shear rate or capillary number.

3.6. Polydisperse Foam. We now consider polydisperse foams composed of three bubble sizes: a_1, a_2, and a_3 for samples H−K and a_1, a_3, and a_4 for samples L−O (see Table 1). Note that in these samples the two larger species always have the same area fraction. Figure 8 shows the steady-state distributions for samples H−K. For sample H with the lowest Φ_3, the largest bubbles (of radius a_3) exhibit a sharply peaked distribution at the center of the gap while the two smaller bubble species (a_1 and a_2) are more or less uniformly distributed. If the a_3 bubbles were absent, the a_1 and a_2 bubbles would not exhibit size segregation as their size ratio $\kappa = 1.43$ is below the threshold for $\Omega = 7$ rpm.[24] Therefore, the aggregation of the a_3 bubbles in sample H is similar to that in a bidisperse foam. By increasing the area fraction Φ_2 and Φ_3 to 10% and 20% (samples I and J), the two smaller bubble species are displaced toward the walls. This is evidently due to the increasing area occupied by the a_3 bubbles at the center and recalls the marginalization of white blood cells when the more flexible red cells aggregate in the center.[22,23]

However, increasing Φ_2 and Φ_3 further to 30% (sample K) brings about an apparent *reversal* of the marginalization. Now, all three species are roughly uniformly distributed in the gap. This can be rationalized by the stronger shear-induced diffusion of the largest bubbles at the higher Φ_3, much as in the bidisperse foams

dx.doi.org/10.1021/la304445f | Langmuir 2013, 29, 1370−1378

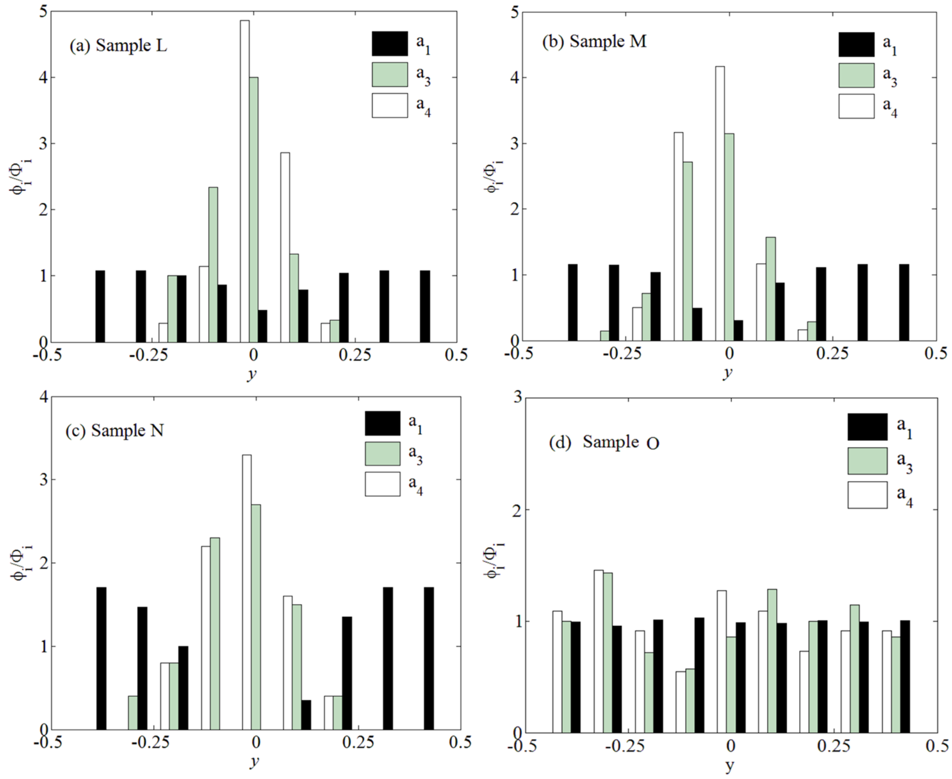

Figure 9. Steady-state bubble distributions in the polydisperse foam samples L, M, N, and O, after 10 min of shearing at 7 rpm. The samples have the same three bubble sizes, $a_1 = 350$ μm, $a_3 = 700$ μm, and $a_4 = 875$ μm, at different area fractions: (a) sample L, $(\Phi_1, \Phi_3, \Phi_4) = (90\%, 5\%, 5\%)$; (b) sample M, (80%, 10%, 10%); (c) sample N, (60%, 20%, 20%); (d) sample O, (40%, 30%, 30%). The area fractions are normalized for each species.

of Figure 5. However, comparing Figures 8 and 5 reveals an interesting role for the a_2 bubbles. In Figure 8d, the a_3 distribution flattens for $\Phi_3 = 30\%$ in the polydisperse sample K, whereas in the bidisperse sample F (Figure 5c), the large bubbles are not quite uniformly distributed even for $\Phi_3 = 50\%$. Thus, the a_2 bubbles are not inert and merely passively displaced by the a_3 bubbles. They actively facilitate the spreading of the largest bubbles. This may have occurred through hindering their migration toward the center (via effectively reducing κ) or enhancing the diffusion of the largest bubbles, or even both.

Now, we investigate the size segregation in polydisperse samples L−O in which the two larger species, a_3 and a_4, both tend to migrate away from the walls and compete with each other to occupy the center of the gap. Figure 9 shows the equilibrium distributions of the three bubble species subject to shearing at Ω = 7 rpm. As it turns out, the two large bubble species behave similarly in this case. For $\Phi_3 = \Phi_4 \leq 20\%$ (samples L−N), both a_3 and a_4 bubbles aggregate at the center of the gap. The a_1 bubbles are marginalized as seen above. The largest a_4 species enjoys a narrower distribution with a higher peak than a_3. Thus, the larger bubble size κ affords the former an advantage. With increasing Φ_3 and Φ_4, the distributions broaden until at 30%, both become more or less uniformly distributed across the gap (sample O). As in Figures 5c and 8d, this can be ascribed to the dominance of the shear-induced diffusion of the a_3 and a_4 bubbles.

4. CONCLUSION

We have studied the structural evolution of bidisperse and polydisperse 2D foams in a narrow-gap Couette shear cell. Within the parameter ranges tested, the main experimental findings can be summarized as follows:

(a) After shearing for a sufficiently long time, the foam achieves a quasi-steady morphology that is independent of the initial configuration.
(b) In this quasi-steady state, the bubble species may be uniformly mixed or segregated by size depending on the physical and flow parameters. Size segregation occurs if the bubble size ratio and shear rate are both above certain threshold values and if the area fraction of the large bubbles is not too high. Otherwise a mixed state is obtained.
(c) In size-segregating bidisperse foams, the segregation occurs more rapidly and produces a narrower final distribution for higher shear rates and larger bubble size ratios. On the other hand, increasing the area fraction of the large bubbles leads to a broader final distribution that is achieved in less time.
(d) Polydisperse foams behave similarly in that size segregation occurs at relatively low area fractions of the largest bubbles while a uniformly mixed morphology prevails at higher large-bubble area fractions. The bubbles of intermediate size tend to facilitate the broadening of the distribution of the largest bubbles.

These observations are rationalized by adapting a migration−diffusion model previously developed for monodisperse emulsions. Viewing the larger bubbles as being suspended in an effective continuum comprising the smaller ones, we describe the structural evolution in bidisperse foams by a convection−diffusion equation. The model balances two competing factors, the lateral migration due to wall repulsion and the shear-induced diffusion due to interaction among the large bubbles. For bidisperse 2D foams, the model predicts all aspects of the experimental observations, often with quantitative accuracy.

The success of the emulsion model in predicting bubble segregation in a polydisperse bubble raft is quite remarkable, especially in view of the differences between the two systems. The prevailing thinking of foam dynamics is that it is determined by the interfacial morphology on the local scale. Then, the 2D foam studied here can be viewed as a curious exception where at least one attribute of the dynamics, the migration and segregation of bubbles based on size, turns out not to be intimately related to the morphology of the smaller bubbles. These small bubbles can be replaced in a sense by an effective continuum while preserving the same segregation of the large bubbles. There are some caveats to this analogy, however. The "replacement" of the surrounding bubbles by an effective continuum is so as to produce the same amount of deformation on the large bubbles. This boils down to an effective capillary number. One cannot reduce the analogy further to something more tangible, say an effective viscosity, which would not produce the correct migration velocity from the Chan–Leal formula (eq 2). Thus, the effective capillary number embodies intricate local dynamics having to do with the discreteness of the surrounding bubbles, which exert a "bumping force" on the large bubbles[24] that cannot be ascribed to an elevated medium viscosity. Moreover, the analogy may be limited to certain types of foam. In our experiment, the bubbles are closely packed but not pressed against one another so as to produce polygonal facets. If we try to pack more bubbles into the raft, they tend to pile on top of others and destroy the two-dimensionality. Thus, the smaller bubbles are essentially undeformed in our experiments. In drier foams that undergo more intensive interaction among bubbles, for example, through T1 events,[3] the continuum analogy may no longer hold.

To conclude, let us briefly return to prior experiments that motivated our study. Our findings suggest that, in the prior experiment of Herzhaft,[13] where 3D polydisperse foams are sheared between parallel plates, shear-induced migration probably has occurred to produce marginalization of smaller bubbles to the plates and a central layer rich in large bubbles. However, three-dimensionality affects how neighboring bubbles interact with one another, and our 2D model will need to be upgraded before it can be compared quantitatively to 3D foam experiments. In addition, it is important to note the experimental and numerical results of Cox and co-workers[18,19] that showed no size segregation in 2D foams undergoing cyclic *planar extension and compression*. The conditions in their studies differ from ours in at least three aspects. In extensional flows, the bubbles do not follow parallel streamlines. Instead, neighboring rows are compressed into one while being elongated in the orthogonal direction. Thus, the interaction among bubbles differs markedly from the rubbing and bumping in our shear experiments. Moreover, the cyclic straining introduces repeated encounters among bubbles, a feature absent from steady shearing. Finally, the maximum extensional rate in their experiments is only 0.0455 s^{-1}, much below our threshold value of 4.17 s^{-1} for approximately the same bubble-size ratio $\kappa = 2$. Their simulation employed the Surface Evolver and is thus quasi-static in nature. Therefore, it appears that size segregation in extensional flows remains an open question that requires further studies, especially at high strain rates.

AUTHOR INFORMATION

Corresponding Author

*E-mail: jfeng@chbe.ubc.ca.

Notes

The authors declare no competing financial interest.

ACKNOWLEDGMENTS

We thank G. M. Homsy and G. Ghigliotti for helpful discussions. The study was supported by NSERC, the Canada Research Chair program, and the Canada Foundation for Innovation.

REFERENCES

(1) Khan, S. A.; Schnepper, C. A.; Armstrong, R. C. Foam rheology: III. Measurement of shear flow properties. *J. Rheol.* **1988**, *32*, 69–92.

(2) Kraynik, A. M. Foam flows. *Annu. Rev. Fluid Mech.* **1988**, *20*, 325–57.

(3) Weaire, D.; Hutzler, S. *The Physics of Foams*; Oxford University Press: Oxford, U.K., 2001.

(4) Lauridsen, J.; Twardos, M.; Dennin, M. Shear-induced stress relaxation in a two-dimensional wet foam. *Phys. Rev. Lett.* **2002**, *89*, 098303.

(5) Katgert, G.; Latka, A.; Mobius, M. E.; van Hecke, M. Flow in linearly sheared two-dimensional foams: from bubble to bulk scale. *Phys. Rev. E* **2009**, *79*, 066318.

(6) Katgert, G.; Tiche, B. P.; Mobius, M. E.; van Hecke, M. Couette flow of two-dimensional foams. *Europhys. Lett.* **2010**, *90*, 54002.

(7) Ritacco, H.; Kiefer, F.; Langevin, D. Lifetime of bubble rafts: cooperativity and avalanches. *Phys. Rev. Lett.* **2007**, *98*, 244501.

(8) Vandewalle, N.; Lentz, J. F. Cascades of popping bubbles along air/foam interfaces. *Phys. Rev. E* **2001**, *64*, 021507.

(9) Biance, A.-L.; Delbos, A.; Pitois, O. How topological rearrangements and liquid fraction control liquid foam stability. *Phys. Rev. Lett.* **2011**, *106*, 068301.

(10) Carrier, V.; Colin, A. Coalescence in draining foams. *Langmuir* **2003**, *19*, 4535–4538.

(11) Debŕegeas, G.; Tabuteau, H.; di Meglio, J.-M. Deformation and flow of a two-dimensional foam under continuous shear. *Phys. Rev. Lett.* **2001**, *87*, 178305.

(12) Dennin, M. Statistics of bubble rearrangements in a slowly sheared two-dimensional foam. *Phys. Rev. E* **2004**, *70*, 041406.

(13) Herzhaft, B. Correlation between transient shear experiments and structure evolution of aqueous foams. *J. Colloid Interface Sci.* **2002**, *247*, 412–423.

(14) Golemanov, K.; Tcholakova, S.; Denkov, N. D.; Ananthapadmanabhan, K. P.; Lips, A. Breakup of bubbles and drops in steadily sheared foams and concentrated emulsions. *Phys. Rev. E* **2008**, *78*, 051405.

(15) Mohammadigoushki, H.; Ghigliotti, G.; Feng, J. J. Anomalous coalescence in sheared two-dimensional foam. *Phys. Rev. E* **2012**, *85*, 066301.

(16) Quilliet, C.; Idiart, M.; Dollet, B.; Berthier, L.; Yekini, A. Bubbles in sheared two-dimensional foams. *Colloids Surf., A* **2005**, *263*, 95–100.

(17) Cantat, I.; Poloni, C.; Delannay, R. Experimental evidence of flow destabilization in a two-dimensional bidisperse foam. *Phys. Rev. E* **2006**, *73*, 011505.

(18) Cox, S. J. The mixing of bubbles in two-dimensional bidisperse foams under extensional shear. *J. Non-Newtonian Fluid Mech.* **2006**, *137*, 39–45.

(19) Vaz, M. F.; Cox, S. J.; Teixeira, P. I. C. Cyclic deformation of bidisperse two-dimensional foams. *Philos. Mag.* **2011**, *91*, 34.

(20) Lyon, M. K.; Leal, L. G. An experimental study of the motion of concentrated suspensions in two-dimensional channel flow. Part 1. Monodisperse systems. *J. Fluid Mech.* **1998**, *363*, 25–56.

(21) Lyon, M. K.; Leal, L. G. An experimental study of the motion of concentrated suspensions in two-dimensional channel flow. Part 2. Bidisperse systems. *J. Fluid Mech.* **1998**, *363*, 57–77.

(22) Shevkoplyas, S. S.; Yoshida, T.; Munn, L. L.; Bitensky, M. W. Biomimetic autoseparation of leukocytes from whole blood in a microfluidic device. *Anal. Chem.* **2005**, *77*, 933–937.

(23) Kumar, A.; Graham, M. D. Margination and segregation in confined flows of blood and other multicomponent suspensions. *Soft Matter* **2012**, *8*, 10536–10548.

(24) Mohammadigoushki, H.; Feng, J. J. Size differentiated lateral migration in sheared two-dimensional foam. *Phys. Rev. Lett.* **2012**, *109*, 084502.
(25) Chan, P. C. H.; Leal, L. G. The motion of a deformable drop in a second-order fluid. *J. Fluid Mech.* **1979**, *92*, 131−170.
(26) Leal, L. G. Particle motions in a viscous fluid. *Annu. Rev. Fluid Mech.* **1980**, *12*, 435−476.
(27) Eckstein, E. C.; Bailey, D. G.; Shapiro, A. H. Self-diffusion of particles in shear flow of a suspension. *J. Fluid Mech.* **1977**, *79*, 191−208.
(28) Leighton, D.; Acrivos, A. Measurement of shear-induced self-diffusion in concentrated suspensions of spheres. *J. Fluid Mech.* **1987**, *177*, 109−131.
(29) King, M. R.; Leighton, D. T. Measurement of shear-induced dispersion in a dilute emulsion. *Phys. Fluids* **2001**, *19*, 397.
(30) Hudson, S. D. Wall migration and shear-induced diffusion of fluid droplets in emulsions. *Phys. Fluids* **2003**, *15*, 1106−1113.